Rocky Worlds DDT: JWST Data Analysis Report for LHS 1140 b

Douglas Long and Taylor J. Bell
JWST Data Analysis Team

October 20, 2026

1 Observation Overview

Under the RWDDT program, JWST-DDT-12498 Observation 2 obtained time-series imaging of LHS 1140 b using MIRI/F1500W with the SUB256 subarray, covering 8.75 hours with the goal of measuring the secondary eclipse of the planet. No attempt is made here to incorporate data from the previous observation to improve measurement of the eclipse depth or timing. High Level Science Products (HLSPs) from this observation are hosted on MAST and include both intermediate and final results to help drive research-community engagement.

We measured both the centroid position and width of the target's point-spread function (PSF) during each integration. The telescope pointing remained quite stable along the x and y axes throughout the observation, but the width of the PSF along both axes increased smoothly during the first ∼1 hour of the observation before settling to a stable value (see Figure 1). A decrease in the raw flux is seen during the first ∼1 hour as well.

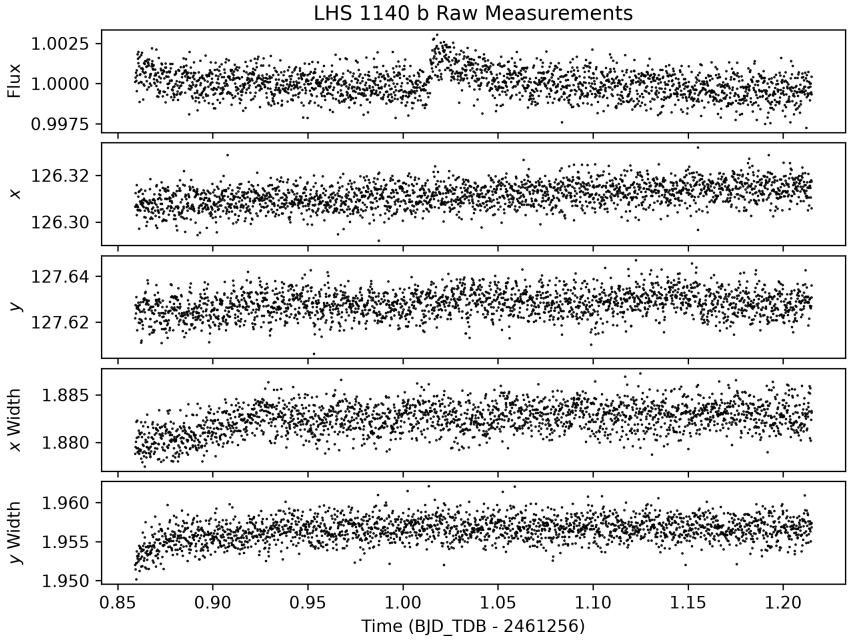

Figure 1: Stability of flux, centroid, and PSF. Time series of changes in the normalized raw flux, centroid position (x, y), and PSF width (computed as a Gaussian standard deviation along the x and y axes), illustrating initial settling behavior, observed stellar flare, and overall pointing stability.

2 Data Reduction

This analysis used the standard JWST pipeline (`jwst` v2.0.1, with CRDS context file `jwst_1535.pmap`) for detector-level calibrations. Stage 1 processing included running the following steps: `saturation`, `lastframe`, `reset`, `linearity`, `rscd`, and `jump` (with the threshold increased from 4.0 to 8.0). In Stage 2 we ran the `flat_field` step, but we disabled the `photom` step as flux-calibrated data are not desired for time-series analyses.

Photometric extraction and light curve fitting were completed using Stages 3–5 of the `Eureka!` Python package (1.5.dev230+g52cf7bef0). A time series was constructed for each pixel, and 3.5σ outliers (along with all `NaN` values) were replaced using bilinear interpolation over the nearest neighbors. Next, a center-of-mass centroid was calculated for each integration using the 'mgmc' method within `Eureka!`'s Stage 3. The position and width of the target's PSF along the x and y axes were measured in each integration using a 2D Gaussian fit (see Figure 1). These measurements were compiled into cotrending vectors that were subsequently used as independent variables in the systematics modeling.

Photometric light curves were extracted in Stage 3 of `Eureka!` using the `photutils` package with circular apertures and 'exact' edges, where pixels are weighted by the fraction of their area lying within the specified aperture. A range of aperture and background annulus radii were considered. Aperture radii ranged from 4–12 pixels, in 1-pixel steps. The inner radius of the background annulus varied from 14 to 30 pixels in 4-pixel steps, while the annulus width ranged from 10 to 40 pixels in 10-pixel steps. Photometric light curves were generated for each source aperture + background annulus pair. In Stage 4, we chose to mask any integrations lying 3.5σ away from the rolling median using a boxcar filter with a width of 21 integrations.

After Stage 4 processing, the presence of a $\sim$1800 ppm bump in the middle of the lightcurve, around 2461257.03 $\mathrm{BJD_{TDB}}$, became evident. An analysis of the guide star telemetry, as well as the analysis of the MIRI centroid and PSF widths (see Figure 1), revealed no changes that coincided with this bump seen in the lightcurve. We attribute this feature to stellar activity, likely a flare from the host star.

3 Light Curve Fitting

The dominant features of the white light curve are the detector settling ramp at the beginning of the observation and the stellar flare near the midpoint of the time series. To reduce the impact of the detector settling, the first 100 integrations were discarded prior to fitting. The light curve was modeled using an eclipse model multiplied by a flare model and a systematic noise model. A Gaussian Process was used to marginalize over the impact of any remaining temporally correlated ('red') noise. The full fitted model can be written as:

$$M(t) = E(t)\,F(t)\,S(t) + GP(t), \tag{1}$$

where $E(t)$ is the eclipse model generated with `batman`, $F(t)$ is the adopted flare model, and $S(t)$ describes the instrumental systematics. The additive $GP(t)$ term is the Gaissian Process. Our priors are summarized in Table 1.

The stellar flare $F(t)$ was fit using an asymmetric Lorentzian profile

$$F(t) = \begin{cases} 1 + \dfrac{A_{\rm F}}{1 + \left(\dfrac{t - t_{\rm F}}{\gamma_{\rm F,LHS}}\right)^2}, & t \leq t_{\rm F}, \\ 1 + \dfrac{A_{\rm F}}{1 + \left(\dfrac{t - t_{\rm F}}{\gamma_{\rm F,RHS}}\right)^2}, & t > t_{\rm F}. \end{cases} \tag{2}$$

where A_F is the flare amplitude, t_F is the flare midpoint, and $\gamma_{\rm F,LHS/RHS}$ is the characteristic width for each side of the profile.

Our systematic model is given by

$$S(t) = P(t)\, R(t)\, X\big(x(t)\big)\, Y\big(y(t)\big)\, SX\big(sx(t)\big)\, SY\big(sy(t)\big), \tag{3}$$

where

$$P(t) = c_0 + c_1(t - \bar{t}) \tag{4}$$

is a linear trend in time and

$$R(t) = 1 + r_0 \exp\left[-r_1(t - t_{\rm start})\right] \tag{5}$$

models the detector settling exponential ramp. The centroid position and PSF width decorrelation terms are each assumed to be linear, for example,

$$X(x) = 1 + c_x(x - \bar{x}), \tag{6}$$

where ($x(t)$, $y(t)$) is the measured centroid position as a function of time, ($sx(t)$, $sy(t)$) is the PSF width along the x- and y-axes as a function of time, ($\overline{x}$, $\overline{y}$) is the time-averaged centroid position, and ($\overline{sx}$, $\overline{sy}$) is the time-averaged PSF size.

The GP used the celerite2 package with a Matérn-3/2 kernel. The kernel is defined as

$$k(t) = \sigma^2 \left[(1 + 1/\epsilon)\; e^{-(1-\epsilon)\sqrt{3}\,t/\rho}\,(1 - 1/\epsilon)\; e^{-(1+\epsilon)\sqrt{3}\,t/\rho}\right],$$

where σ^2 and ρ control the amplitude and the length scale of the covariance, respectively. ϵ determines the approximation to a true Matérn-3/2 function. The default of $\epsilon = 0.1$ was used.

All model parameters were sampled simultaneously using the `dynesty` dynamic nested sampling algorithm. We used an initial 136 live points with the 'rwalk' sampling algorithm and the 'multi' bounds and an initial $d \log \mathcal{L} < 0.01$ stopping criterion. Subsequent batches of 68 live points were then iteratively added with `pfrac` set to 0.5 (balancing the improvement in the precision of the posterior and evidence) until the default stopping criterion was achieved.

3.1 Results & Discussion

The results of our fits are summarized in Table 1. We find an eclipse depth -26^{+70}_{-61} ppm at the time predicted for a circular orbit, which is consistent with a non-detection of the eclipse in this analysis. This fitted eclipse is just after the start of a strong flare with a much larger amplitude of 1816^{+123}_{-120} ppm, and it is likely that different approaches to the flare modeling could produce very different eclipse depths.

Table 1: The astrophysical and systematic model priors for the fits assuming a circular orbit. Fixed astrophysical parameters are shown without uncertainties and are taken from the juliet$_{circ}$ fit from the CIT's orbit fitting efforts during observational scheduling. Gaussian priors are shown as $\mathcal{N}(\mu, \sigma)$ with mean μ and standard deviation σ, while Uniform priors are shown as $\mathcal{U}(l, u)$ with lower-limit l and upper-limit u.

Parameter	Prior	Posterior
P (days)	24.7372456564	–
$t_{\rm sec}$[‡] (BMJD$_{\rm TDB}$)	58411.79895773	–
b	0.1416126966	–
a/R_*	95.2031220450	–
e	0	–
$R_*/R_\odot$[†]	0.2159	–
$R_{\rm p}/R_*$	0.0743630409	–
$F_{\rm p}/F_*$ (ppm)	$\mathcal{N}(91, 200)$	-26^{+70}_{-61}
$A_{\rm F}$ (ppm)	$\mathcal{U}(0, 5000)$	1816^{+123}_{-120}
$\gamma_{\rm F,LHS}$	$\mathcal{U}(0, 0.1)$	$0.00074^{+0.00046}_{-0.00043}$
$\gamma_{\rm F,RHS}$	$\mathcal{U}(0, 0.1)$	$0.02241^{+0.00327}_{-0.00273}$
$t_{\rm F}$ (BMJD$_{\rm TDB}$)	$\mathcal{N}(61256.52, 0.05)$	$61256.51537^{+0.00060}_{-0.00074}$
c_0	$\mathcal{N}(0.999, 0.01)$	$0.999841^{+0.000190}_{-0.000139}$
c_1	$\mathcal{N}(0.0, 0.1)$	$-0.00190^{+0.00053}_{-0.00083}$
r_0	$\mathcal{N}(0.00, 0.01)$	$0.00086^{+0.00023}_{-0.00022}$
r_1	$\mathcal{U}(3, 300)$	178^{+74}_{-76}
c_y	$\mathcal{N}(0.0, 0.5)$	$0.0004^{+0.0028}_{-0.0029}$
c_x	$\mathcal{N}(0.0, 0.5)$	$0.0037^{+0.0032}_{-0.0033}$
c_{sy}	$\mathcal{N}(0.0, 0.5)$	0.031 ± 0.011
c_{sx}	$\mathcal{N}(0.0, 0.5)$	0.033 ± 0.011
A	$\mathcal{U}(-24, -10)$	$-17.63^{+2.83}_{-1.86}$
m	$\mathcal{U}(-7, 0)$	$-1.96^{+1.31}_{-3.73}$
scatter_mult	$\mathcal{U}(0.8, 10)$	1.173 ± 0.018
Residual Std. Dev. (ppm)	N/A	729 ± 11

[†]The stellar radius is used to account for the difference in light travel time throughout the planet's orbit.
[‡]Due to the large flare's proximity to the expected eclipse, $t_{\rm sec}$ was fixed.

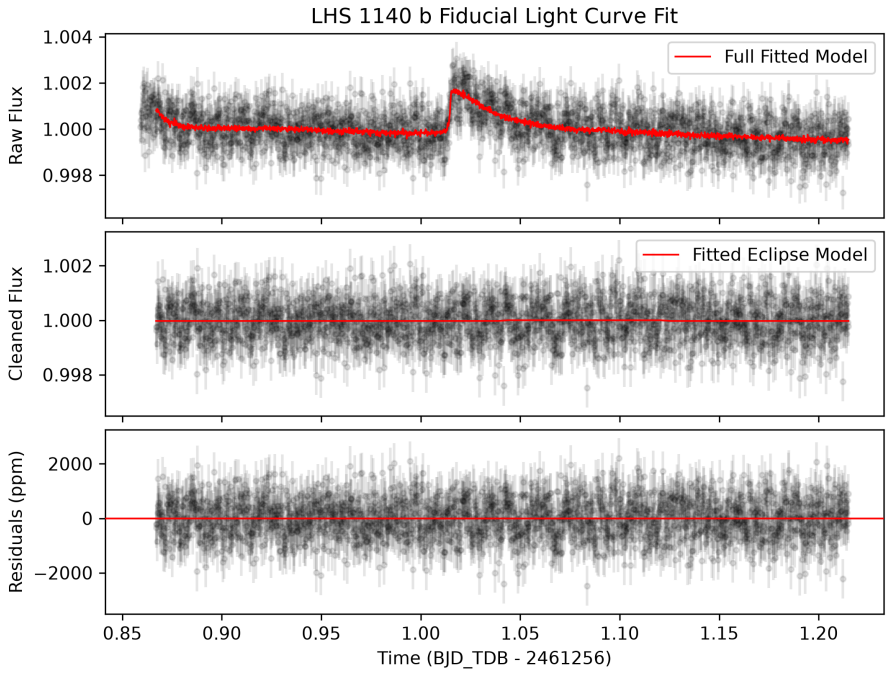

Figure 2: Fiducial light curve fit. *Top:* Raw, normalized flux measurements in black with (systematic × eclipse × flare + GP mean predictive model) over-plotted in red. The first 100 integrations were not included in the fit. *Middle:* Systematics-divided (and flare-removed) flux measurements are shown in black, with the eclipse model shown in red. *Bottom:* "Data − model" residuals.

4 Calibrated Stellar Flux Measurement

Following the methodology of Gordon et al. (2025), we measured absolutely-calibrated stellar photometry using `calints` FITS files with a 5.69 px aperture and an 8.63–11.45 px background annulus, applying an aperture correction of 1.497. Adding in quadrature the observational scatter with the $\sigma(\mathrm{CF}) = 0.48\%$ and $\sigma(\mathrm{repeat}) = 0.45\%$ terms from Gordon et al. (2025), we obtained a calibrated stellar flux of 9.181 ± 0.060 mJy using the out-of-eclipse and out-of-flare baseline.

5 Discussion and Outlook

This report presents the analysis of the second RWDDT JWST eclipse observation of LHS 1140 b. No statistically significant eclipse signal was detected in these data. Instead, the dominant feature is a ∼1800 ppm peak, assumed to be a stellar flare occurring just prior to the expected eclipse. No anomalies are seen in the MIRI centroid positions or PSF at that time, making it unlikley to be due to an instrument problem.

A similar flare was seen in Observation 1, so we used the same approach of fitting an asymmetric Lorentzian profile to the light curve. Still, the magnitude of the flare prevents a reliable measurement of the eclipse depth from this observation alone. Additional eclipse observations will be needed to disentangle stellar variability from the planetary signal and place meaningful constraints on the thermal emission of LHS 1140 b.